BABEȘ-BOLYAI UNIVERSITY

Faculty of Physics

Doctoral School of Physics

Ordering of block copolymers in thin films processed via advanced solvent vapor annealing

Abstract

by

Iulia BĂBUȚAN

A thesis submitted in fulfilment of requirement for the degree

DOCTOR OF PHILOSOPHY in PHYSICS

Scientific Coordinator:

C.S.I Dr. Habil. Ioan BOTIZ

Cluj-Napoca

2025

Keywords: block copolymers, thin films, solvent vapor annealing, self-assembly, atomic force microscopy, polymer crystallization, synthetic antimicrobial polymers, assembled nanostructures, surfaces and coatings, antimicrobial properties, spin-casting.

Abstract

Polymers play an important role in the realization of most technological applications, which have a significant influence on the development of our society and life system. Whether it is the automotive or aeronautical industry, packaging materials and adhesives, insulating and optoelectronic applications, medical devices and antibacterial or drug delivery solutions, environment and cosmetics, in all these broad research fields polymers play an important role. The key connection establishing the main properties of polymeric systems and their related properties is the microstructure-processing-property relationship. In this doctoral thesis, we propose to process several novel diblock- and triblock copolymer systems, and eventually to drive them into puzzling, highly ordered hierarchical structures.

To begin with, we have developed an efficient processing technique that would help achieve the proposed objectives, namely to manipulate and modify the microstructure of the above-mentioned materials. This technique is based on a novel and advanced space confined solvent vapor annealing method, able to process and optimize the microstructure of various block copolymers under the action of solvent vapors. The lamellar and micellar characteristics, such as lamellar/particle size and the type of resulting morphologies were further correlated with the length of a polymer chain or the interaction coefficients, and

further analyzed to understand the newly generated block copolymer architectures/microstructures. The goal of this process was to self-assemble the block copolymers into periodic lamellar or hexagonal microstructures of molecular dimensions. Thus, for each type of polymer system, specific microstructures were obtained under very unique experimental conditions.

More precisely, the processing method we developed is based on the deposition through condensation of a large amount of solvent vapors on the surface of thin block copolymer films. For that, block copolymer films were heated to 40 °C, at a rate of 0.3 °C/s, followed by a cooling of the film to 12-15 °C, also at a rate of 0.3 °C/s. At such lower temperatures, solvent vapors condensed and block copolymer films were swollen-rich and turned into quasi two-dimensional "film-solutions" where polymer molecules were completely dissolved. By slowly heating the films back to 40 °C, this time at a much lower rate of 0.01 °C/s, the solvent was gradually evaporated, allowing polymer molecules to self-assemble or crystallize in highly ordered, often hierarchical structures. The study was first carried out on diblock- and triblock copolymers, and generated periodic lamellar and hexagonal ordered morphologies, respectively.

We further used our newly developed space confined solvent vapor annealing method to process block copolymers in different types of solvents. Results have shown that the obtained ordered structures depended on how volatile and good the utilized solvent was and on how long were the blocks of each block copolymer system.

The same processing method was applied to polymer systems that were composed inclusively of a crystallizable block in their composition, in order to also favor the crystallization process. Such a block, a key component of a diblock- or triblock-copolymer, led to the generation of highly crystalline microstructures, especially when the number of crystallizable monomers was sufficiently high. In

some cases, crystallization could be observed already in thin films obtained right after spin-casting, without being subsequently processed by exposure to solvent vapors in a space confined sample chamber.

Table of Contents

Introduction

The here presented doctoral thesis discusses the scientific path we have taken regarding the latest state-of-the-art research on processing of diblock- and triblock-copolymers (di- and tri-BCPs) in thin films. These copolymers are mainly used in the medical field, especially for obtaining medical materials such as prostheses, implants, but also in industry for fabricating lubricants, paints, etc. Due to the importance given to them in the medical field, we decided to deepen the research and to design and develop an efficient processing method capable to self-assemble and/or eventually to crystallize such BCPs into highly ordered (crystalline) structures.

The doctoral thesis is structured in five well-organized chapters. In terms of content, each chapter addresses a specific theme. Thus, they do not only relate to the overall picture of what a BCP means and its uses, but also propose a completely new, state-of-the-art, yet highly effective method for processing such polymers, so that the surface microstructure for such materials can be manipulated and adjusted.

In chapter one, a general overview of what polymers are and their uses is presented, this being the only theoretical chapter. In other words, it gives us information on important aspects about these compounds and further provides the most relevant scientific achievements regarding the related processing-microstructure-properties relationship, as well as the applications of such polymers. Furthermore, it also shows the various methods utilized to fabricate thin films and process polymers, inclusively the method proposed by us: the

exposure of thin polymeric films to rich amounts of solvent vapors in a relatively confined space, a method we called solvent vapor annealing in a quasi-confined environment (C-SVA).

In the second chapter, the di- and tri-BCP systems used throughout the scientific research are discussed. Here, the state-of-the-art homemade device that we used to process these polymers is described in detail, along with other characterization techniques that we used to evaluate the quality of the obtained structures. Furthermore, we shortly described the synthesis method of the polymers used and the operating parameters for the fabrication of thin films and further processing methods used, including the C-SVA.

In chapter three, we have described the use of C-SVA on various di-BCPs. Basically, relatively large amounts of solvent vapors were condensed on the surface of the thin film through C-SVA, with the goal to pursuit their self-assembly into ordered, periodic lamellar or hexagonal nanostructures of molecular size, depending on the type of BCP used. The results provided by atomic force microscopy (AFM) indeed demonstrated that the surfaces of thin films obtained from the polymeric system of poly(2-vinylpyridine)-*b*-polybutadiene and processed via C-SVA were comprised of periodic lamellar morphology. Meanwhile, the surfaces of thin films spin-cast from poly(2-vinylpyridine)-*b*-poly(cyclohexyl) methacrylate) and further processed via C-SVA led to the formation of a hexagonally packed morphology. These microstructures were generated on solid substrates for the first time.

Next, in chapter four, using C-SVA, we have exposed thin films of di- and tri-BCPs to large amounts of distinct types of solvent vapors, aiming again to obtain their self-assembly into ordered structures. From the results provided by the AFM, exposure of thin films of poly(4-vinylpyridine)-*b*-polybutadiene, poly(2-vinylpyridine)-*b*-polybutadiene and poly(2-vinylpyridine)-*b*-poly(tert-butyl methacrylate)-*b*-poly(cyclohexyl methacrylate) BCPs led to the formation of

both periodic lamellar nanostructures of molecular lateral dimension and micellar structures that were further organized either into superstructures composed of parallel stripes or honeycomb-like configurations.

In the last chapter, five, we show how thin films spin-cast from tri-BCP polybutadiene-*b*-poly(2-vinylpyridine)-*b*-poly(ethylene oxide) and exposed to solvent vapors using the C-SVA method underwent crystallization process. Following the analysis of the results obtained by optical microscopy and AFM, we have demonstrated that the as spin-cast thin films containing a short crystallizable poly(ethylene oxide) block led to crystallization, and thus to highly ordered crystals of dendritic shapes, only after processing in solvent vapors through the C-SVA method. In contrast, thin films spin-cast from tri-BCPs containing a larger poly(ethylene oxide) crystallizable chain led to the formation of dendritic crystalline structures inclusively immediately after the spin-casting process. Interestingly, further exposure to solvent vapors has accentuated the formation of such crystalline structures.

Last but not least, the thesis ends with the general conclusions and perspectives we have envisioned for the near future, followed closely by the list of references and few annexes. The latter contain all the publications that formed the basis of this study, thus strictly related to this thesis, as well as the conferences where the doctoral candidate presented her results.

Chapter 1

Basic notions on the BCP self-assembly and crystallization processes and resulting ordered/crystalline structures

1.1 Self-assembly of AB-type di-BCPs

We will discuss the self-assembly of AB-type BCP in organic solvents, as well as the micellar characteristics obtained during self-assembly in polar and non-polar solvents, including solvent mixtures. First, we will discuss the self-assembly of AB-type copolymers that also include crystallizable sequences. Figure 1.1.1 shows the main primary micellar morphologies such as spheres, cylinders and vesicles. It is important to emphasize, however, that the formation of these distinct morphologies is strongly influenced by the intrinsic molecular features of the copolymers, the nature of the solvent environment, as well as the specific conditions under which micellization occurs.

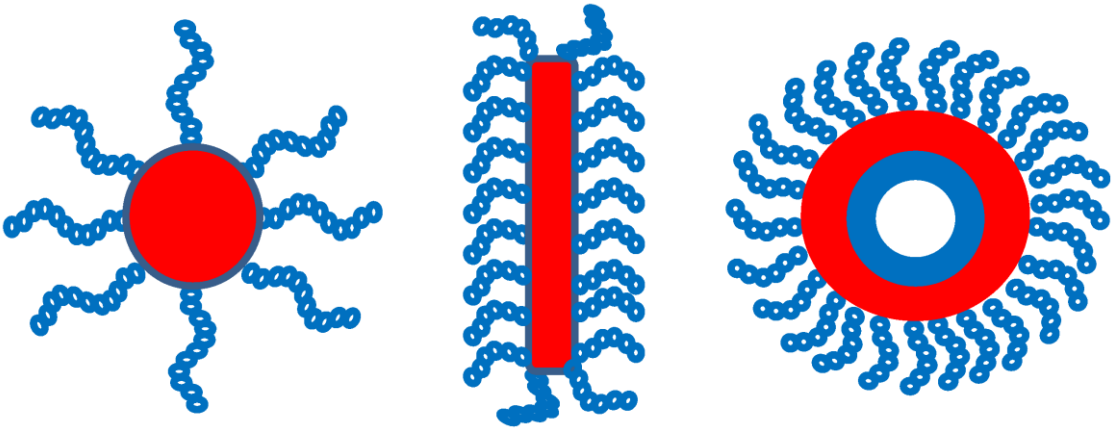

Spherical micelle **Rod-like micelle** **Vesicle**

Figure 1.1.1. The main basic morphologies for AB-type BCPs. This image was reproduced with permission from ref. [1].

Another important aspect is that an amphiphilic copolymer of type AB, in a certain solvent specific for blocks A and B, can usually form two types of morphologies, having either an A or a B micellar core. As demonstrated by Li and coworkers, this inversion of the micellar structure can be induced by a thermal treatment for the self-assembly of copolymers of the type poly(tert-butylmethacrylate)-*b*-poly[*N*-(4-vinylbenzyl)-*N*,*N*-diethylamine] (P*t*BMA-*b*-PVEA) in methanol [2], an aspect represented schematically in Figure 1.1.2. Thus, for the P*t*BMA-*b*-PVEA BCP, it was found that at the lower critical solution temperature (LCST), T = 60 ℃, the micelles are inverted and have a diameter of 42 nm, while at the upper critical solution temperature (UCST), T = 5 ℃, the micelles recorded a diameter of 53 nm [2].

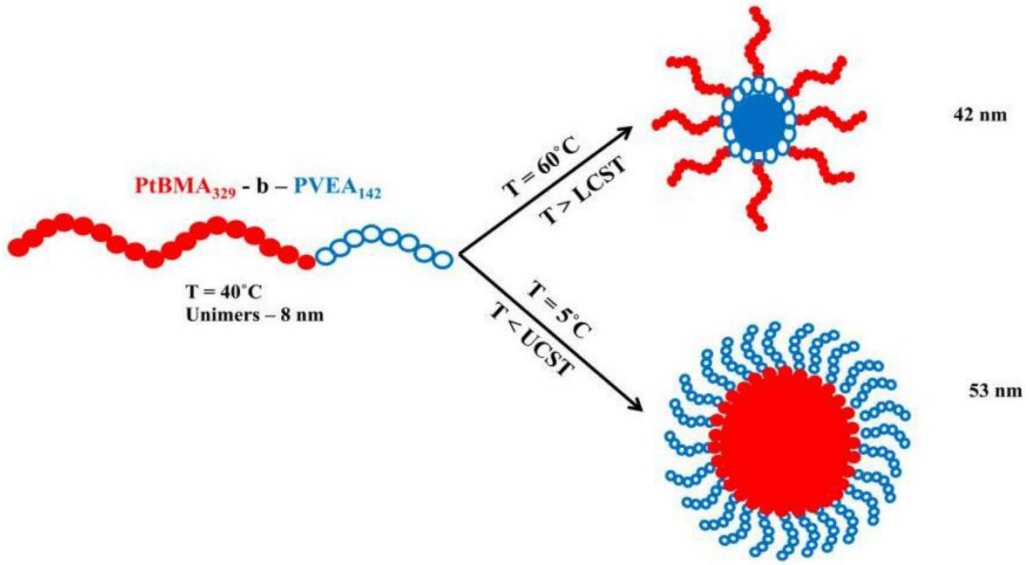

Figure 1.1.2. Main micellization characteristics of the P*t*BMA$_{329}$-*b*-PVEA$_{142}$ BCP in methanol. This image was reproduced with permission from ref. [1].

1.2 Self-assembly of ABC tri-BCPs

Another category of BCPs that was utilized to develop micellar structures are the ABC tri-block terpolymers. This statement is being highlighted in numerous works in the literature [3], [4], [5]. Over the years, many studies on the self-assembly of ABC copolymers have shown the formation of micelles in aqueous media, while only a relatively small number have reported the obtaining of micelles in organic solvents. Many researchers, including Wyman and Liu [5], but also Gröschel and Müller [6] have demonstrated the numerous morphologies that can be obtained for a given ABC copolymer, either in a given solvent or in mixtures of solvents. Thus, according to the study carried out by Wyman and Liu [5], the main spherical micellar morphologies of ABC tri-block terpolymers are shown in Figure 1.2.1 where the solvent selectivity is also taken into account. To date, the influence of self-assembly according to the sequences of tri-block terpolymers has been demonstrated in aqueous media [7], [8], and in water/organic solvent mixtures [9].

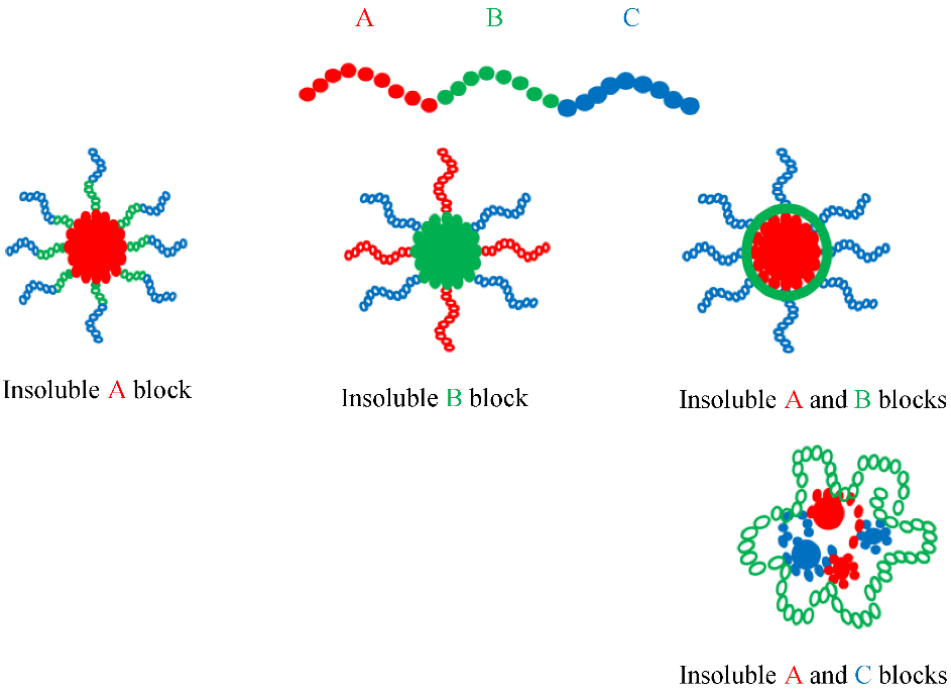

Figure 1.2.1. Main morphologies for lamellar ABC-type tri-BCPs. This image was reproduced with permission from ref. [1].

Chapter 2

Materials and Methods

2.1 Polymeric systems

In this PhD thesis we used several polymer systems such as poly(4-vinylpyridine)-*b*-polybutadiene ($P4VP_{34}$-*b*-PB_{207}, $P4VP_{43}$-*b*-PB_{70}), poly(2-vinylpyridine)-*b*-polybutadiene ($P2VP_{37}$-*b*-PB_{188}), poly(2-vinylpyridine)-*b*-poly(tert-butyl methacrylate)-*b*-poly(methacrylate cyclohexyl) ($P2VP_{107}$-*b*-P*t*BMA_{52}-*b*-$PCHMA_{604}$, $P2VP_{25}$-*b*-P*t*BMA_{12}-*b*-$PCHMA_{173}$), poly(acrylic acid)-*b*-poly(cyclohexyl methacrylate)-*b*-poly(acrylic acid) (PAA_{31}-*b*-$PCHMA_{207}$-*b*-PAA_{31}), polybutadiene-*b*-poly(2-vinylpyridine)-*b*-poly(ethylene oxide) (PB_{100}-*b*-$P2VP_{100}$-*b*-PEO_{104}, PB_{185}-*b*-$P2VP_{108}$-*b*-PEO_{154}, PB_{348}-*b*-$P2VP_{252}$-*b*-PEO_{697}, PB_{66}-*b*-$P2VP_{69}$-*b*-PEO_{356}), poly(2-vinylpyridine)-*b*-poly(cyclohexyl methacrylate) ($P2VP_{181}$-*b*-$PCHMA_{643}$) and poly(cyclohexyl methacrylate)-*b*-poly(acrylic acid) ($PCHMA_{520}$-*b*-PAA_{214}). These systems are di- and tri-BCPs with numerical average molecular weights of M_n= 14.800 g/mol, 8.400 g/mol, 14.100 g/mol, 120.000 g/mol, 33.300 g/mol, 39.200 g/mol, 20.500 g/mol, 28.200 g/mol, 76.000 g/mol, 26.400 g/mol, 108.000 g/mol, 102.800 g/mol. This can be better visualized in Table 2.1.1. The synthesis process was carried out by anionic polymerization in THF in the presence of n-butyllithium (n-BuLi) at -75 ℃. Details on the synthesis can be found in previous studies, as they were published by our collaborators [10], [11].

Table 2.1.1. Dimensions of di- and tri-BCP thin films before and after exposure to solvent vapors. This table has been reproduced with permission from refs. [12], [13], [14], [15].

Block-copolymer	Molecular weights (g/mol)	Solvent type	Film thickness (nm)
$P4VP_{34}$-*b*-PB_{207}	14.800	chloroform	~ 105
$P4VP_{43}$-*b*-PB_{70}	8.400	chloroform	~ 95
$P2VP_{37}$-*b*-PB_{188}	14.100	toluene	~ 97
$P2VP_{107}$-*b*-P*t*BMA_{52}-*b*-$PCHMA_{604}$	120.000	THF	~ 106
		1,4 - dioxane	~ 106
		toluene	~ 106
$P2VP_{25}$-*b*-P*t*BMA_{12}-*b*-$PCHMA_{173}$	33.300	1,4 - dioxane	~ 99
PAA_{31}-*b*-$PCHMA_{207}$-*b*-PAA_{31}	39.200	1,4 – dioxane	~ 112
		THF	~ 112
PB_{100}-*b*-$P2VP_{100}$-*b*-PEO_{104}	20.500	toluene	-
PB_{185}-*b*-$P2VP_{108}$-*b*-PEO_{154}	28.200	toluene	32±3
PB_{348}-*b*-$P2VP_{252}$-*b*-PEO_{697}	76.000	toluene	23±5
PB_{66}-*b*-$P2VP_{69}$-*b*-PEO_{356}	26.400	toluene	18±3
$P2VP_{181}$-*b*-$PCHMA_{643}$	108.000	1,4 - dioxane	~ 103
$PCHMA_{520}$-*b*-PAA_{214}	102.800	1,4 - dioxane	-

The structural representations of the BCPs used in this study are shown in the images presented in Figure 2.1.1.

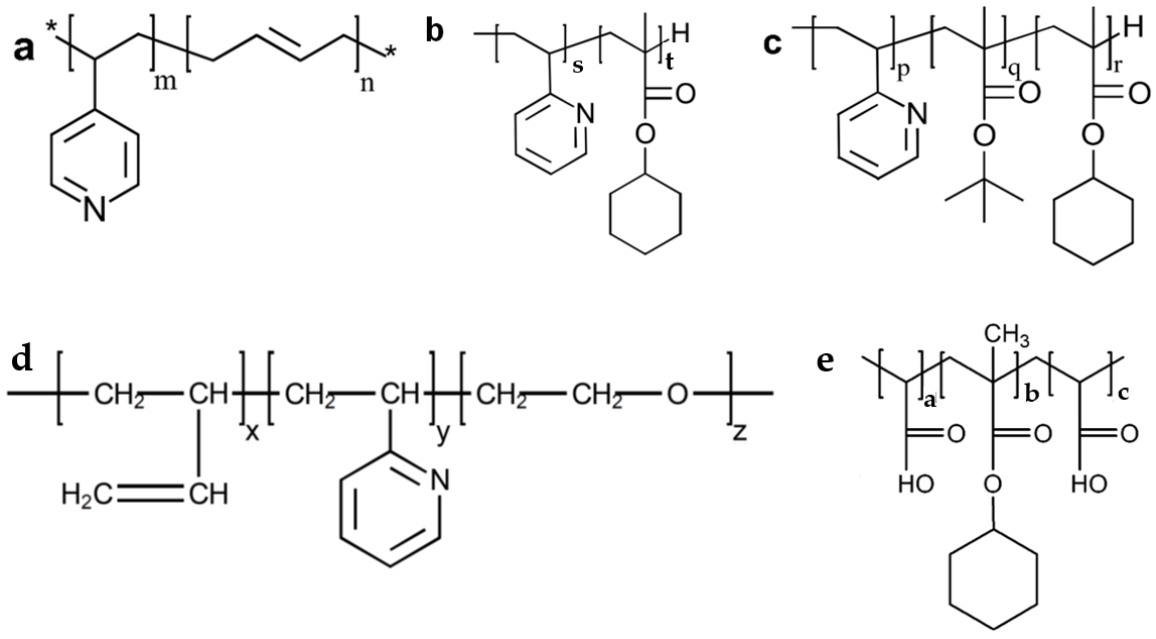

Figure 2.1.1. Structural formulas of the main BCPs used in our study, P4VP-*b*-PB (a), P2VP-*b*-PCHMA (b), P2VP-*b*-P*t*BMA-*b*-PCHMA (c), PB-*b*-P2VP-*b*-PEO (d), PAA-*b*-PCHMA-*b*-PAA (e). Here, the subscripts represent the number of repeating monomer units corresponding to each polymer system used (m is 34, 43 or 37, n takes the values 207, 70 or 188, s is 181, and t 643, p can be 107 or 25, q is 52 or 12, r takes the values 604 or 173, x represents 100, 185, 348 or 66, y can be 100, 108, 252 or 69, and z replaces 104, 154, 697 or 356, a takes a single value 31, the same for b which is 207, and c will be 31). This image has been reproduced with permission from references [13], [14], [15].

2.2 Methods used to fabricate and process thin BCP films

2.2.1 Spin casting thin films of di- and tri-BCPs

The di- and tri-BCPs thin films of different thickness (see Table 2.1.1, above) were obtained by casting the copolymer solutions on a glass and silicon substrates (WS-650mz23nppb, Laurell Technologies Corporation, North Wales, PA, USA), a process carried out at a speed of 2000 rpm for 30 seconds. The thickness of each BCP film was determined by applying a fine scratch on the surface of the respective film, and then measuring the depth of the scratch profile with the AFM technique. The entire process of fabricating thin films by the spin-casting method is shown in the image in Figure 2.2.1.1. The information provided in this section has been adapted according to the materials and methods section of our paper published in the ref. [14].

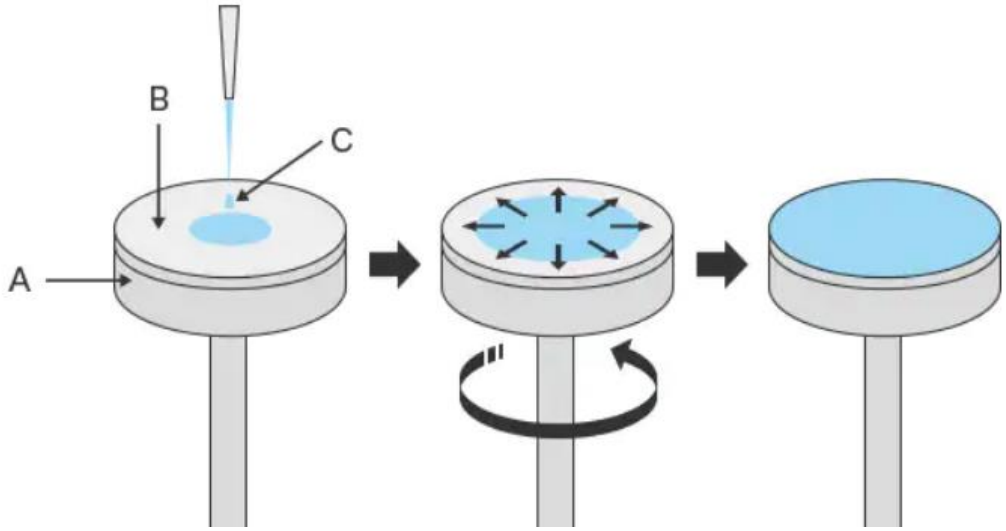

Figure 2.2.1.1. Scheme for obtaining thin films on silicon wafers by spin-casting technique (A – Rotary stage, B – Target surface, C – Coating fluid). Reproduced with permission from ref. [16].

2.2.2 Processing of thin films of di- and tri-BCPs by using the C-SVA method

For the processing of as spin-cast BCP thin films by exposure to solvent vapors in a closed environment via C-SVA, we used a homemade configuration consisting of a small aluminum chamber, equipped with a Peltier module with a role in heating and cooling the bottom of the sample chamber, and thus, the sample (15.4 V/8.5 A from Stonecold). The temperature of the Peltier module, which is actually the initial temperature of the sample, is regulated using a controller (TCM U 10A from Electron Dynamics Ltd., Southampton, UK), whose feedback is given by a PT100 temperature sensor located inside the chamber next to the sample. This PT100 sensor continuously transmits the temperature inside the chamber to the temperature controller, which then changes the direction of the electric current within the Peltier element depending on the need to heat or cool the system (the power supply is 12 V/10A). However, it must be taken into account that on the other side of the Peltier module there is a radiator and a fan, with a role in equalizing the temperature difference. Next, the controller is connected to a

computer software that provides access to setting the sample temperature with an accuracy of 0.01 ℃ and maintaining it constant as long as it is needed. Solvent vapors enter the sample chamber, where the sample is located, through a system consisting of a nitrogen-driven bubbler, as represented in the schematic model in Figure 2.2.2.1. The actual configuration of the handmade C-SVA device is shown in the images in Figure 2.2.2.2.

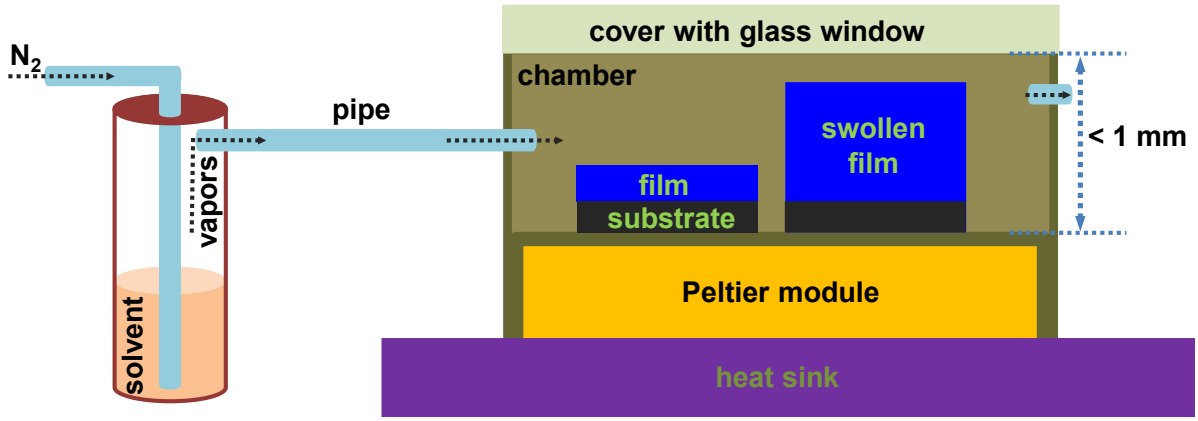

Figure 2.2.2.1. Schematic representation of the installation used for the processing of BCP thin films. The Peltier module was connected to a temperature controller and a PT100 sensor, which helped regulate the temperature, and the radiator was further coupled to a fan. Solvent vapors entered the sample processing chamber through a pipe previously connected to a nitrogen-based bubbling system, as illustrated on the left. The scheme also shows the thin film before (left) and after (right) it was exposed to solvent vapors. It should be also noted that the dimensions shown in the diagram are only indicative and do not reflect the actual size of the assembly. This figure was reproduced with permission from ref. [14].

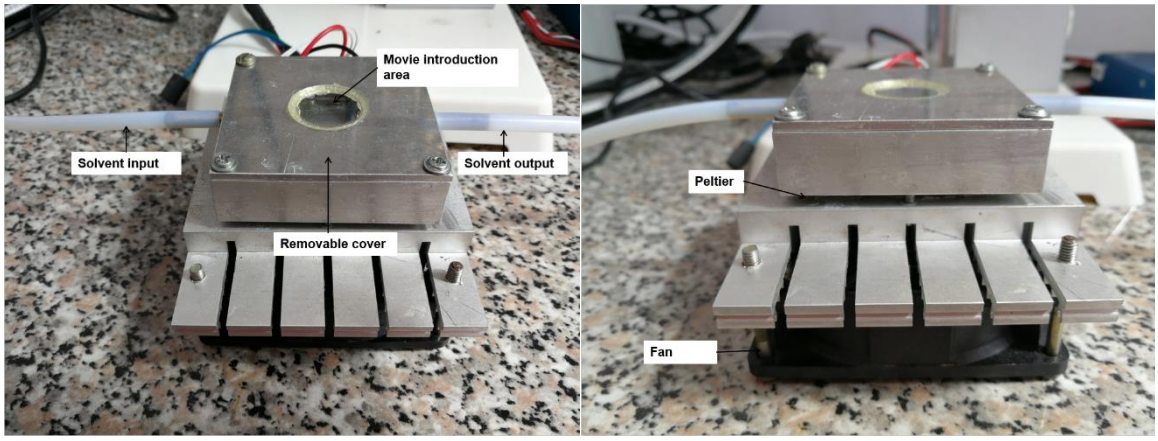

Figure 2.2.2.2. Photographs depicting C-SVA handmade system used to process thin films of various BCPs.

The amount of solvent vapor introduced into the sample chamber is regulated with a flowmeter attached to the nitrogen bubbler. The thin film once introduced into the sample chamber is heated to approximately 40 °C. Meantime, a regulated amount of solvent vapor is introduced into the chamber. We will then set the temperature to 15 °C. As the temperature decreases at a rate of 0.3 °C/s, around a temperature of 23 °C solvent vapors begin to condense on the surface of the BCP film, and the latter begins to swell. As a result of this process, interference colors begin to be observed in terms of film color changes, associated with the increase in film thickness (at this point, it is understood that each film color corresponds to a specific film thickness, an aspect deduced from the AFM measurement of the sample and presented in details in previous dedicated studies [17], [18]). Thus, at around 15 °C we observed that enough solvent has been condensed on the film surface, as we have already a quasi 2D "film-solution" with a polymer concentration (C_P) of approximately 5%. It should be specified that the film concentration was determined as the ratio between the thickness of the initial film obtained by spin-cast and the one exposed to solvent vapor at a specific sample temperature (note here that the initial film thickness was determined by AFM measurements through fine film scratching). For the

processed film, the interface color was taken into account to establish the thickness (in this case the thickness of such a film reached approximately 2 μm; again, more details on the procedure thickness calibration procedure with the help of AFM can be found in previous studies [17], [18]). We maintained the sample in this state for about 1 minute, after which we reversed the process and started increasing the sample temperature, at a much lower rate of 0.01 ℃/s, precisely to allow the BCP molecules to start packing into highly ordered nanostructures, until we gradually reach 40 ℃ again.

Once the process of temperature increase has been initiated, the solvent vapors that have been deposited on the surface of the thin film started to gradually evaporate, and the BCP film slowly returned to its initial thickness, but its microstructure was significantly altered/modified. Generally, even weak gradients in temperature may generate huge variations in film thickness upon swelling. Therefore, such gradients were always avoided, by setting the C-SVA tool to reach each temperature set point gradually and smoothly. The entire experimental set-up is presented in Figure 2.2.2.3. It is worth noting that part of the materials and methods section has been adapted from the publication in references [13] and [14].

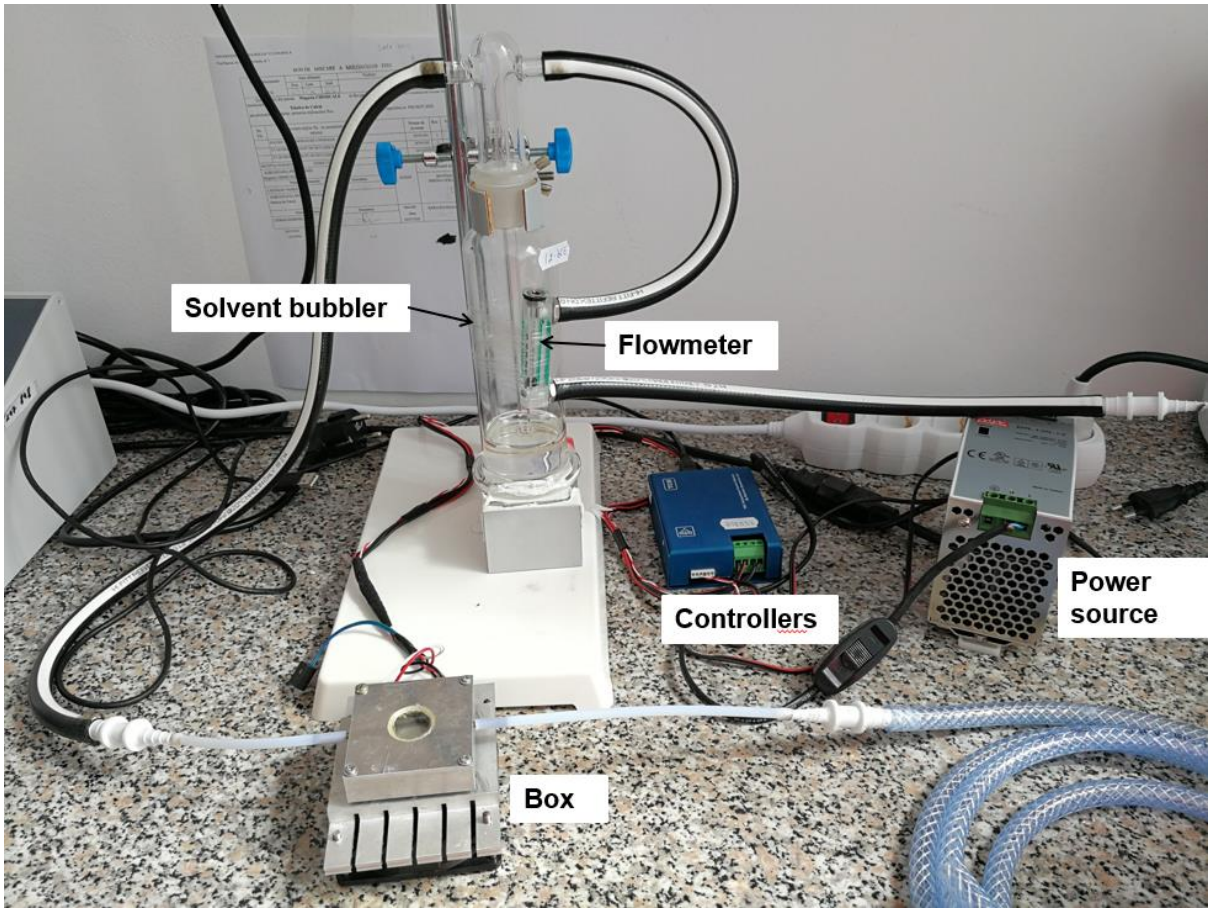

Figure 2.2.2.3. Photograph depicting the whole film structuring system used to process thin BCP films via C-SVA.

Chapter 3

Self-assembly of BCP thin films induced through their exposure to large amounts of solvent vapors using the C-SVA method

3.1 Generation of highly ordered lamellar or hexagonal structures in BCP thin films using the C-SVA method

Figure 3.1.1 shows a comparison of the surface of a BCP film obtained by the spin-casting technique and one obtained by exposure to solvent vapors processed by the C-SVA method. All thin films were evaluated using the AFM. After analyzing the obtained results, it was found that the film exposed to chloroform vapors via C-SVA presented periodic parallel stripes on its surface (Figure 3.1.1a), while the film that was not exposed to solvent vapors presented a surface covered with randomly oriented structures of irregular shape (Figure 3.1.1b). These aspects could be observed in more detail thanks to the topographical images with a higher magnification obtained with the AFM and highlighted in Figure 3.1.1c,e and Figure 3.1.1d,f. Thus, the film processed by the C-SVA method presented self-assembled parallel stripes composed of dark domains alternating with light ones, with a periodicity of approximately 23.2 nm (Figure 3.1.1i). Each darker and lighter domain had an average width of approximately 11.6 nm. It is likely that the dark domains corresponded to the PB block with a softer, rubbery texture and

a T_g of less than 90℃ [19], while the lighter, harder domains represented the P4VP block, whose T_g is known to be approximately 142 ℃ (Figure 3.1.1e,g) [20]. In contrast to the film that exhibited a periodic lamellar morphology, the as spin cast reference film that was not processed via C-SVA exhibited disordered structures randomly distributed on the surface (Figure 3.1.1f,h,j) (this paragraph was adapted with permission from ref. [12]).

The size of a vinyl pyridine (VP) monomer is about 25 nm [21], and the extended length of the P4VP block containing 34 monomer units is about 8.5 nm. This value can be compared with the width of the domains provided by the AFM measurements. Thus, it was deduced that the PB blocks were interspersed among the P4VP ones [22]. Such structures were observed by us for the first time. Some recent studies have shown that the PB-*b*-P4VP polymer chains can self-assemble into disk-shaped micelles in the organic phase or into sheet aggregates in the inorganic phase [23]. Moreover, additional studies reported in the literature showed that lamellar structures were obtained only for the tri-BCPs like P4VP-*b*-PB-*b*-P4VP [24], respectively polystyrene-b-polybutadiene-b-poly(4-vinylpyridine) PS-*b*-PB-*b*-P4VP [25]. For di-BCPs, ordered lamellar structures were reported only for the PS-*b*-P4VP system [26] (this paragraph was adapted with permission from ref. [12]).

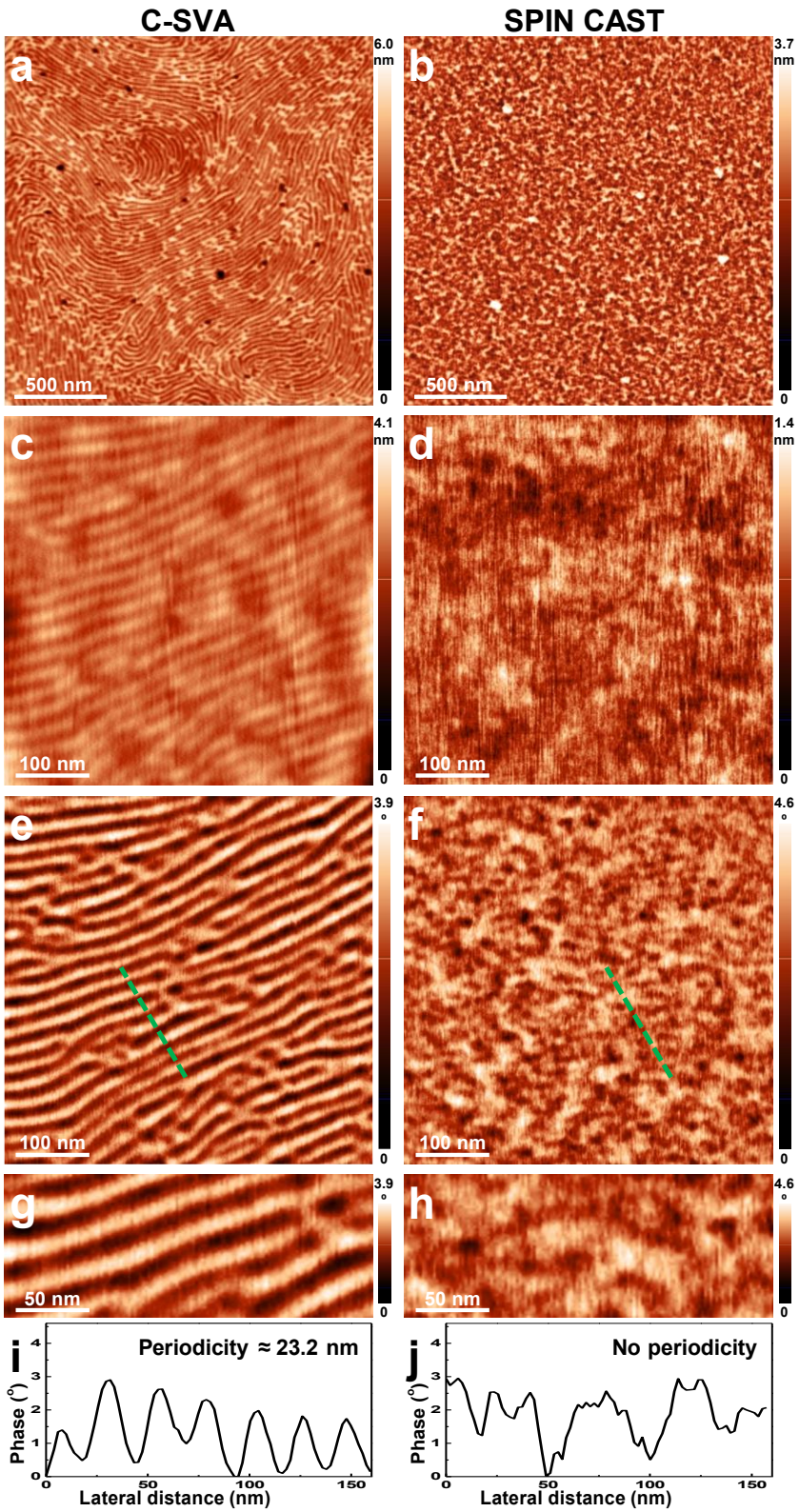

Figure 3.1.1. (a-h) AFM images of height (a-d) and phase (e-h) representing the surface of a film spin-casting from P4VP$_{34}$-*b*-PB$_{207}$ after (a, c, e, g) and before (b, d, f, h) being exposed via C-SVA to chloroform vapors. The region described in (a) can be seen in

the height image (c), while for (b) the magnification is shown in (d). Images (e) and (f) are represented by the magnifications of the micrographs (g) and (h). (i-j) Cross-sections of the profile corresponding to the dashed lines indicated in (e) and (f), where the lateral dimensions measured after (i) and before (j) exposure of the film to solvent vapors are underlined. This figure was reproduced with permission from ref. [12].

3.2 Generation of ordered structures on the surface of thin films of di- and tri-BCPs with altered molecular weights

Figure 3.2.1 shows a comparison of AFM images of thin films made of $P2VP_{37}$-*b*-PB_{188} di-BCP by the spin-casting method and further exposed to solvent vapors using the C-SVA method. The results obtained for the film that was not exposed to solvent vapors show a featureless, but a smooth surface topography, where a surface roughness of approximately 0.1 nm was recorded (Figure 3.2.1b,d). In contrast, the film exposed to solvent vapors showed periodic parallel stripes on its surface, and a roughness of less than 0.3 nm (Figure 3.2.1a,c). However, after examining the phase images (Figure 3.2.1e-h), it was concluded that the very ordered lines observed on the surface of the film exposed to solvent vapors had a periodicity of approximately 13.3 nm (Figure 3.2.1g,i). Similarly, the as spin-cast reference film exhibited random structures possessing no specific shape (Figure 3.2.1h,j). If we look in more detail at Figure 3.2.1g, it will be observed that the parallel light regions alternate with the dark ones, and the average width is less than 7 nm, measured in different regions of the sample. According to the literature, the dark domains correspond to the PB block with a soft texture [24] and the T_g below 90 ℃ [19], and the lighter domains correspond to the P2VP block which is known to have a stiffer texture and T_g around 104 ℃ [20]. Therefore, in the film obtained by the C-SVA method, according to the observed morphology, the P2VP chains were not completely stretched. This was expected, as toluene was

not one of the best solvents for the P2VP block [27], [28]. In contrast, for the PB block the result was exactly the opposite [29], [30]. The favoring interactions of toluene with the PB block, also expressed by the interaction parameters that vary between 0.38 and 0.45, but also by the molecular weight of the PB block [30], promoted ordering of PB chains [29]. While other studies reported in the literature have shown that a variety of structures such as spherical, cylindrical or parallel stripes micelles, or vesicles [31], with ordered lamellar morphologies being reported only for different di- or tri-BCPs containing P2VP (such as PS-*b*-P2VP, P4VP-*b*-P2VP, PMMA-*b*-P2VP, P2VP-*b*-PHIC-*b*-P2VP) [32], [33], [34], [35], [36], [37]), this was the first time when lamellar morphologies were demonstrated for a P2VP-*b*-PB BCP system in thin films. Moreover, we have demonstrated that the width of the lamellar domains of $P2VP_{37}$-*b*-PB_{188} was 13.3 nm, a value smaller compared to the lateral dimension of 23 nm measured for lamellae generated in previous section for the di-BCP $P4VP_{34}$-*b*-PB_{207} [12]. This difference is most probably related to the blocks lengths, i.e., to the shorter length of the PB block in the $P2VP_{37}$-*b*-PB_{188} system (this paragraph was adapted with permission from ref. [13]).

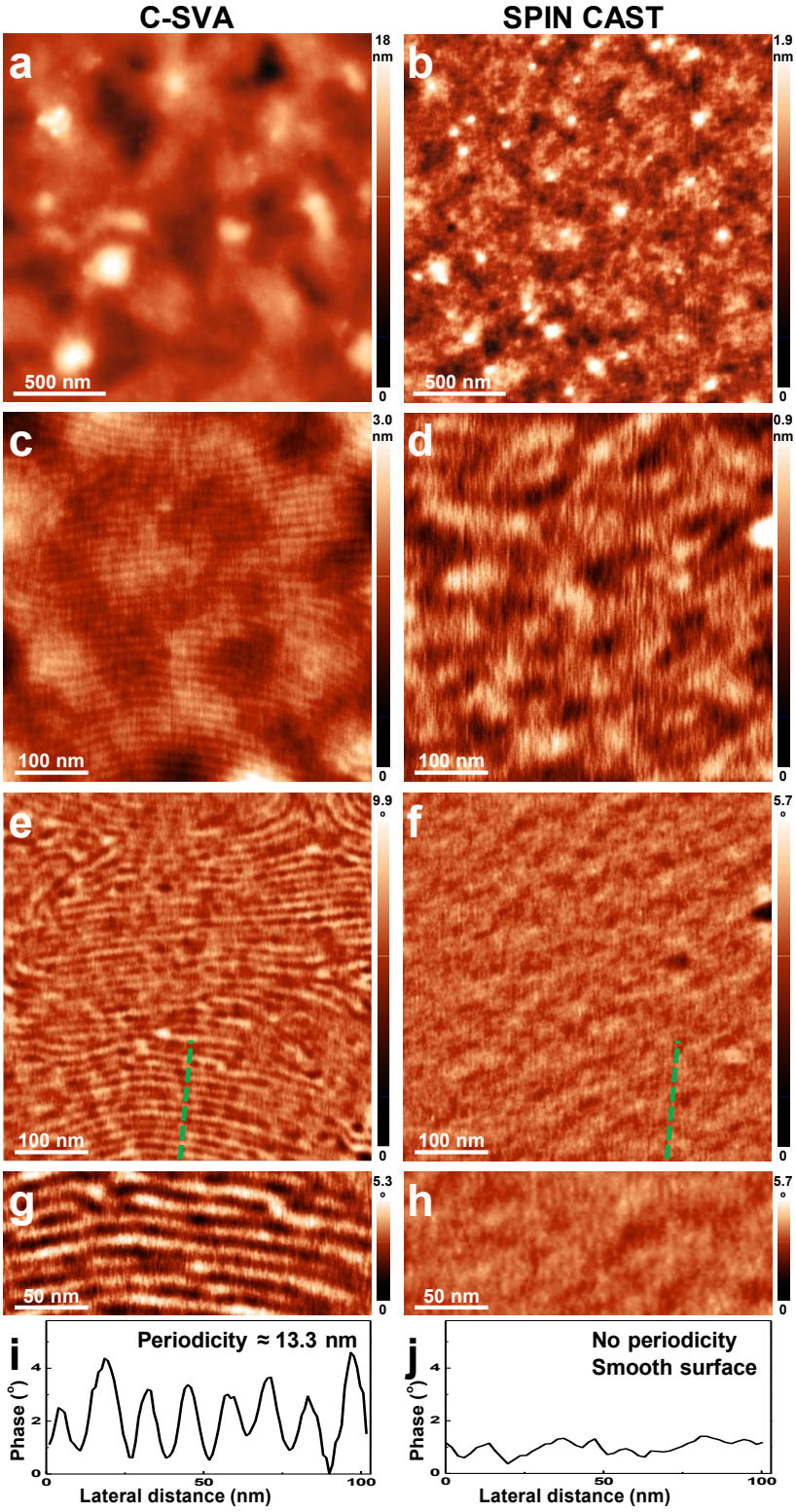

Figure 3.2.1. AFM height (a-d) and phase (e-h) micrographs illustrating the morphologies observed on the surface of a P2VP$_{37}$-*b*-PB$_{188}$ thin film after (a, c, e, g) and before (b, d, f, h) its exposure to toluene vapor. Region (a) is shown at a larger scale in

height micrograph (c) and phase (e). Region depicted in (b) is also shown in micrographs (d) and (f). Images in (e) and (f) are illustrated at a larger scale in micrographs (g) and (h). (i-j) Representation of the cross-section corresponding to the dotted lines indicated in (e) and (f) and highlighting the lateral dimensions measured after (i) and before (j) exposure of the thin film to toluene vapor. This figure was reproduced with permission from ref. [13].

Chapter 4

AFM investigation of the self-assembly of lamellar and micellar BCPs exposed to rich amounts of solvent vapors

4.1 Generation of highly ordered structures in thin films of di- and tri-BCPs through their exposure to distinct types of solvent vapors

Figure 4.1.1 shows the AFM images of thin films spin-cast from $P4VP_{34}$-*b*-PB_{207} di-BCP before and after being exposed to three distinct types of solvent vapor using the well-established C-SVA method. The AFM results showed that after exposure of the $P4VP_{34}$-*b*-PB_{207} film to chloroform vapors, smooth, highly ordered structures covered the entire surface. These structures were composed of periodic parallel stripes, with an average lateral periodicity of approximately 23 nm (Figure 4.1.1a-c). These parallel stripes were further comprised of darker domains alternating with lighter ones. Here, while the former correspond to the softer PB blocks, the latter correspond to the P4VP blocks. Moreover, these domains were formed following the lamellar microphase separation process that inserted the PB blocks between the P4VP domains. In comparison, the analogue film that was not exposed to chloroform vapors (Figure 4.1.1d,e) presented a smooth surface, entirely covered with featureless/shapeless structures. When we replaced the chloroform solvent with 1,2-dichloroethane (1,2-DCE), similar results were obtained (Figure 4.1.1f-h), with the difference that the long parallel stripes turned

out to be exhibiting a more pronounced curvature, as it can be clearly seen by comparing Figure 4.1.1b with Figure 4.1.1g. Nonetheless, when we further replaced 1,2-DCE with a mixture derived from THF and methanol, the situation changed completely, as can be seen in Figure 4.1.1k-m. In this case, it was observed that the parallel stripes have lost their periodicity, leading to a disturbed, much less ordered morphology (Figure 4.1.1i,j and Figure 4.1.1n,o). The clearly distinct quality of the surface morphology in terms of ordering observed for the three solvent types could be explained by taking into account the quality of each solvent used in relation to the two blocks composing the BCP system. In other words, we have considered the Flory-Huggins interaction parameter χ, which measures the interaction of the polymer chains with the solvent molecules, but also the interaction between the two polymeric blocks, i.e., polymer-polymer interaction. If χ is less than 0.5 [38], then the compounds are considered to be miscible. Instead, if χ is greater than 0.5 [38] the compounds are considered to be phase separated. For example, a small interaction parameter χ = 0.022 [39] existing between PB and chloroform indicates that chloroform is a good solvent for this block, facilitating the generation of structures through rather favorable interactions. In such a case, the molecular conformations are expected to be more extended, possibly fully extended in ideal cases. Similarly, such favorable interactions are also expected for the P4VP-chloroform system, in which case χ = 0.443 [40]. Given the incompatibility between the two P4VP and PB blocks, phase separation of the P4VP-*b*-PB system treated with chloroform vapors, yielding ordered lamellar structures is highly efficient (Figure 4.1.1a-c). Other studies have shown that 1,2-DCE is a good solvent for both blocks, PB and P4VP [41], [42], [43], as demonstrated by the interaction parameter χ between PB and 1,2-DCE is 0.425 [39]. In Figure 4.1.1f-h it is observed that $P4VP_{34}$-*b*-PB_{207} BCP formed periodic parallel stripes. Furthermore, even though methanol is a good solvent for P4VP, in which case χ is 0.474 [40], it is nonetheless a very bad solvent

for the PB block (χ = 2.694) [39]. By mixing methanol with a good solvent such as THF (χ is 0.167 between THF and PB block) [39] turns into a poor mixture for the P4VP$_{34}$-*b*-PB$_{207}$ BCP. This means that after processing a film of P4VP$_{34}$-*b*-PB$_{207}$ by using the C-SVA method, ordered structures should not be obtained, which indeed was true as demonstrated in Figure 4.1.1k-m). These results obtained for films exposed to 1,2-DCE and THF/methanol mixture were never published until now (this paragraph was adapted with permission from ref. [12], [13], [15]).

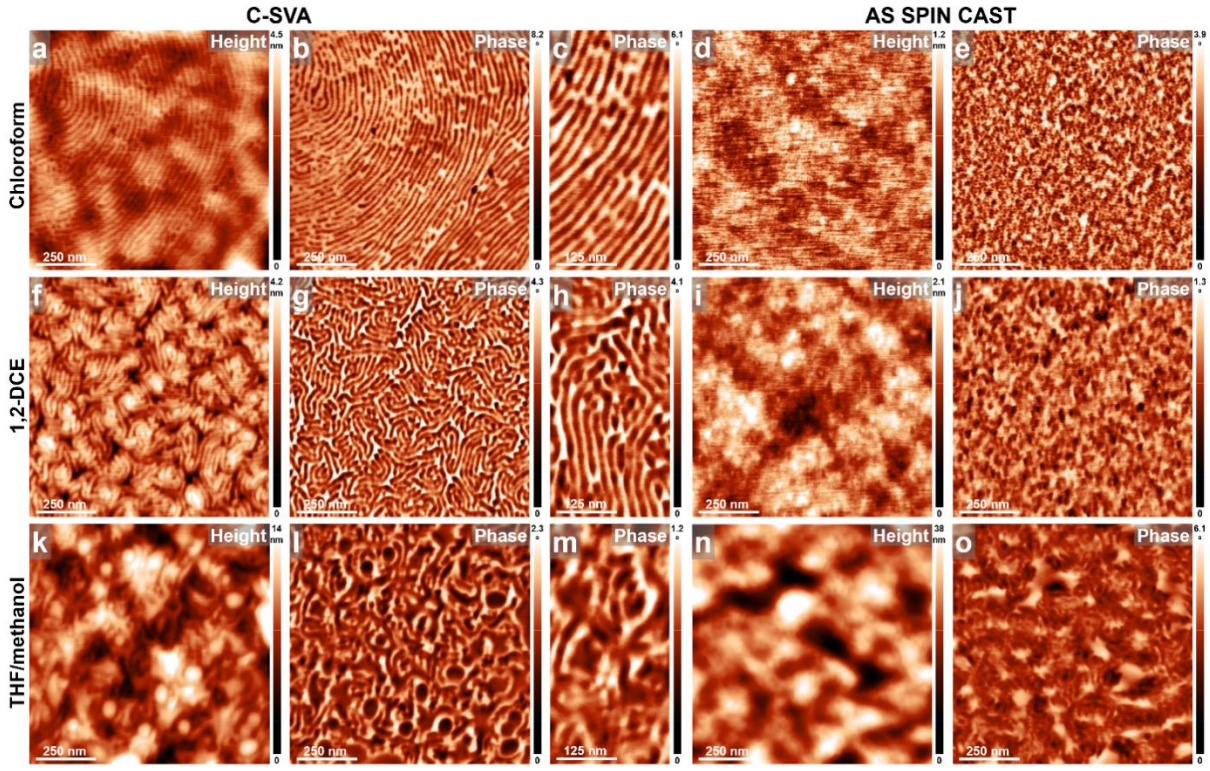

Figure 4.1.1. (a-o) AFM height and phase micrographs showing the surface morphology of thin films made of P4VP$_{34}$-*b*-PB$_{207}$ di-BCP system using spin-casting from chloroform (a-e), 1,2-DCE (f-j) and THF/methanol (k-o) solutions, before (d, e, i, j, n, k-o) and after (d, e, i, j, n, k-c, f-h) their further exposure to the corresponding solvent vapors via C-SVA. This figure was reproduced with permission from ref. [15].

When the number of P4VP blocks was increased to 43 monomers and the PB blocks decreased to 70 monomers, a resulting P4VP$_{43}$-*b*-PB$_{70}$ system was obtained. Thin films were then spin-cast from this di-BCP by spin casting. These films were further exposed to chloroform and THF/methanol vapors, respectively. The obtained AFM results have shown that the entire film surfaces in both cases were covered in a very smooth manner with micelles of an average diameter of 16.7±3 nm, while displaying a roughness of 1.1 nm (Figure 4.1.2a-c and Figure 4.1.2f-h). Considering the values of χ between chloroform and the two blocks of the BCP, we could conclude that the PB block represented the outer part (corona) of the micelles, while the P4VP block formed their core. But when we exposed the system to vapors of the THF/methanol mixture, we expect the situation became exactly the opposite, that is, the P4VP block represented the corona, and the PB block generated the core. Moreover, when we analyzed the analogue reference film spin-cast from chloroform solution that was not exposed to solvent vapors (Figure 4.1.2d,e), we have observed that its corresponding surface was covered entirely with a scaly-like layered morphology. The same morphology was also observed for the reference P4VP$_{43}$-*b*-PB$_{70}$ film that was generated by spin-casting from THF/methanol solution (Figure 4.1.2i,j).

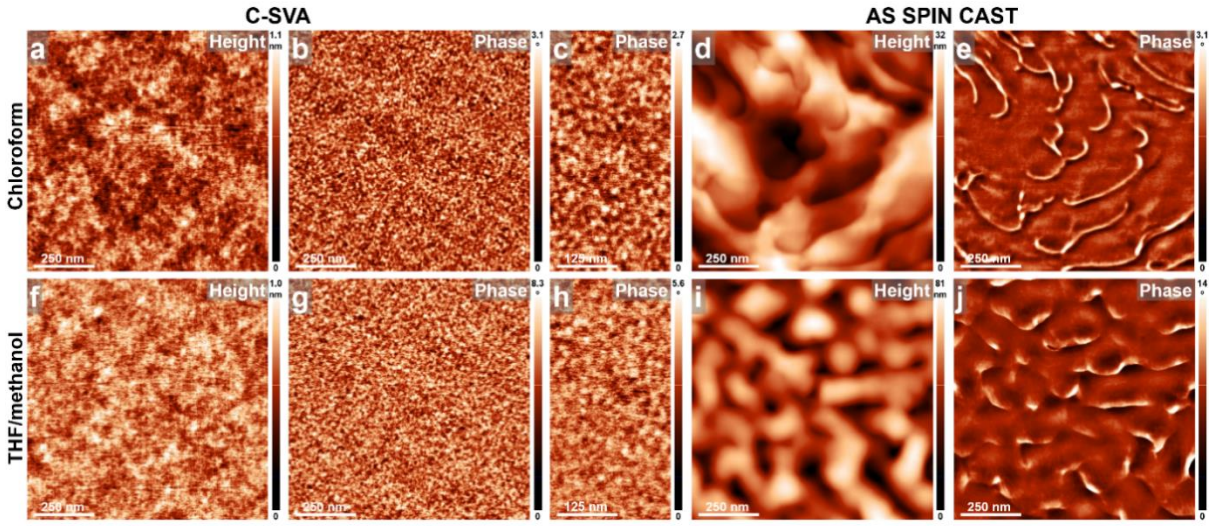

Figure 4.1.2. (a-j) AFM height and phase micrographs showing the surface morphology of thin films for the P4VP$_{43}$-*b*-PB$_{70}$ BCP system generated by spin-

casting from chloroform (a-e) and THF/methanol (f-j) solutions, before (d, e, i, j) and after (a-c, f-h) their exposure to corresponding solvent vapors via C-SVA. This figure was reproduced with permission from ref. [15].

Chapter 5

Crystallization of tri-BCPs based on poly (ethylene oxide) by exposure to solvent vapors using the C-SVA method

5.1 Generation of highly ordered crystalline structures in thin films made of di- and tri-BCPs containing a crystallizable block

The main objective of this study is to highlight the impact of the C-SVA method on the crystallization process of thin films made of di- and tri-BCPs containing a crystallizable block. To successfully achieve this objective, we first used a PB_{100}-*b*-$P2VP_{100}$-*b*-PEO_{104} tri-BCP system [44]. Due to the rather short length of the PEO block of 104 monomers, compared to the lengths of the other two PB and P2VP blocks, which each have 100 monomers, this system is expected to encounter serious difficulties in crystallization, i.e. it is not expected to nucleate and thus to form single crystals or other highly ordered/crystalline structures. Indeed, it was found that crystallization of thin PB_{100}-*b*-$P2VP_{100}$-*b*-PEO_{104} films at temperatures below 40 °C could not be achieved in melt (prior to this, the film was annealed to a temperature of 67 °C to be melted). Also, crystallization cannot proceed under high-speed spin-casting conditions typically that generates on flat surfaces rather disordered morphologies due to fast solvent evaporation. The above statement can be confirmed by the results presented in Figure 5.1.1. From the optical micrograph in Figure 5.1.1b it can be seen that no crystals were formed following the process of spin-casting from PB_{100}-*b*-

$P2VP_{100}$-*b*-PEO_{104} solutions dissolved in toluene. Generated morphology was composed of only irregular and random structures, as indicated by the yellow arrows. From the AFM images shown in Figure 5.1.1d,f, it was clear that brightly colored objects measuring up to few tens of micrometers in length that were visible on the film surface in Figure 5.1.1b were some aggregated structures. The latter were surrounded by irregular domains randomly covering the entire surface. These domains were bright-colored, exhibited a height of a few tens of nanometers, and were surrounding some "empty" and dark-colored irregular regions (Figure 5.1.1d,f). As in the AFM phase images in Figure 5.1.1h, these regions appeared brighter, it was concluded that they could be made of stiffer material, possibly of aggregated or crystalline nature. The higher domains highlighted by lighter colors in Figure 5.1.1f were instead made up a soft and amorphous material. Moreover, as seen in Figure 5.1.1j, some circular nanostructures measuring in average less than 50 nm could also be observed.

In comparison, the thin BCP PB_{100}-*b*-$P2VP_{100}$-*b*-PEO_{104} film processed using the C-SVA method, i.e., exposed to toluene vapors, was covered with large single crystals randomly distributed on the surface, and possessing a dendritic structure (Figure 5.1.1a,c, and Figure 5.1.2a). These results demonstrate that large dendritic crystals could be obtained despite the fact that the crystallizable PEO block was short in comparison to the length of the other two block taken together, and thus well obstructed by the other two blocks. Moreover, the dendritic crystals depicted in Figure 5.1.2a nucleated and grew during the C-SVA processing, within the range of 17–20 ℃ while the concentration of polymer was increasing from about 20% to around 40%. It is important to notice that the four crystals numbered in their centers are "deformed" due to their partial coalescence.

All experimental information obtained by C-SVA and AFM techniques revealed that dendritic crystalline structures were formed exclusively when the chains of the PB_{100}-*b*-$P2VP_{100}$-*b*-PEO_{104} tri-BCP had a high mobility in a dilute, almost quasi-2D "film-solution" regime. This behavior was not observed during

thermal annealing, where the chain mobility was considerably lower than in solution, or during the spin-casting process, where the molecular mobility decreased sharply with the rapid evaporation of the solvent [45].

It was evident that the formation of dendritic crystals resulted from the partial alignment and, most likely, folding of the PEO-type molecular chains, i.e. their crystallization process. The growth process associated with these crystals was, most likely, influenced by a transport mechanism that directed molecules from the vicinity to the crystallization zone (this phenomenon being generally determined by the concentration of polymers in richly swollen "film-solutions" and, implicitly, by the macromolecular diffusion rate [45]).

In addition, this crystallization process could also be influenced by the rate with which PB_{100}-*b*-$P2VP_{100}$-*b*-PEO_{104} chains would attach to a growing crystal. Given that the dendritic structures formed over a few minutes, during which the film temperature slowly increased from approximately 17 ℃ to 20 ℃ (with an extremely low heating rate of 0.01 ℃/s), in a regime where the chains likely possessed high molecular mobility favoring diffusion, we concluded that the probability of attachment of these chains to the growing crystal was rather high and possibly governed by the so-called diffusion-limited aggregation mechanism, which ultimately led to the dendritic morphology [45] (this paragraph was adapted with permission from ref. [14]).

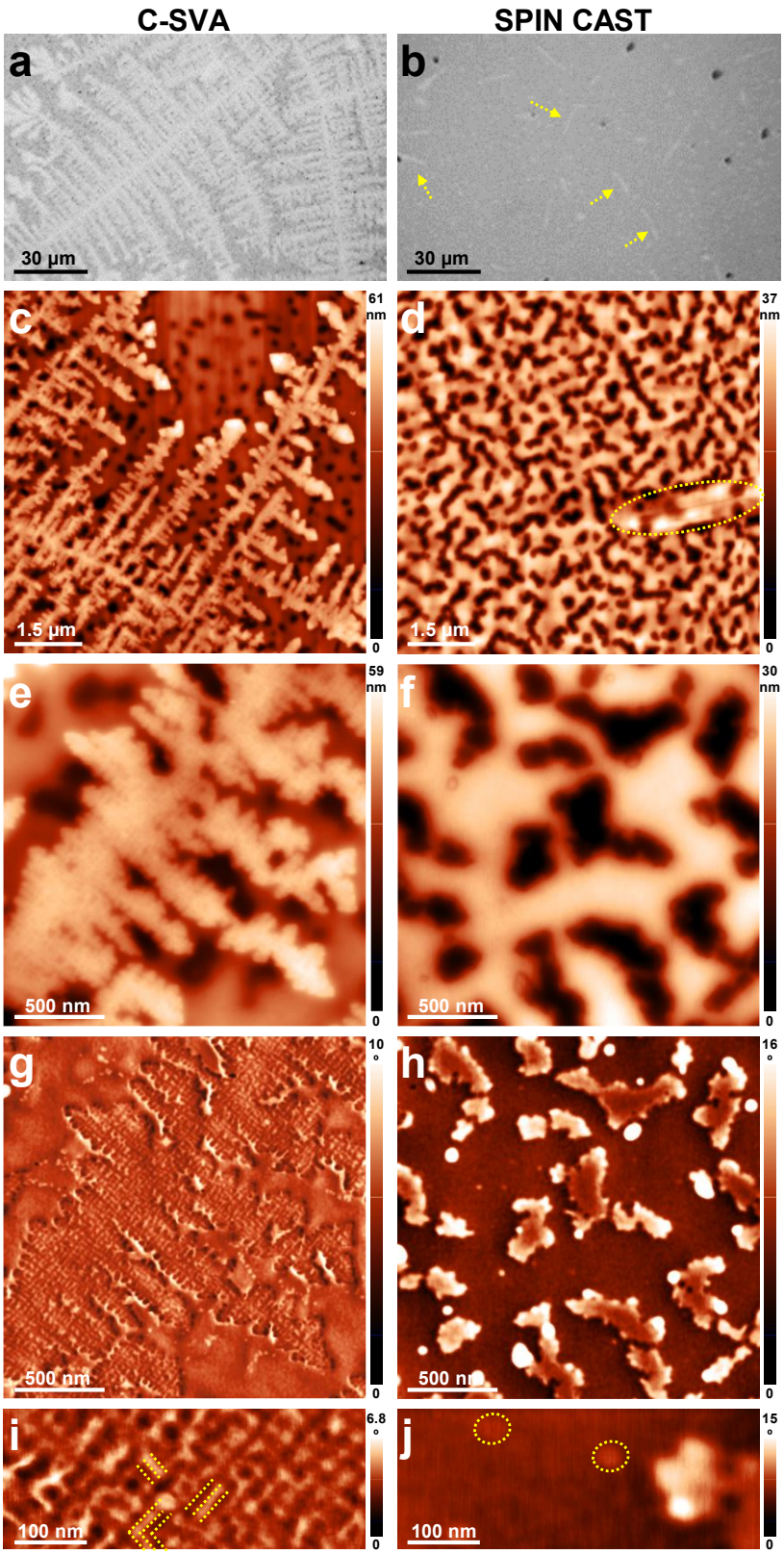

Figure 5.1.1. Optical micrographs (a-b) and AFM height (c-f) and phase (g-j) images depicting the microstructures generated the surface of a PB_{100}-*b*-$P2VP_{100}$-*b*-PEO_{104} thin

film after (a, c, e, g, i) and before (b, d, f, h, j) its exposure to toluene vapors via the C-SVA method. The region shown in (c) is further depicted in higher magnification in height (e) and phase (g) images shown in (e, g). Similarly, the region illustrated in (d) is further shown in (f) and (h). The images shown in (i) and (j) represent an enlargement of the images shown in (g) and (h), respectively. The arrows are for guidance only. This figure was reproduced with permission from ref. [14].

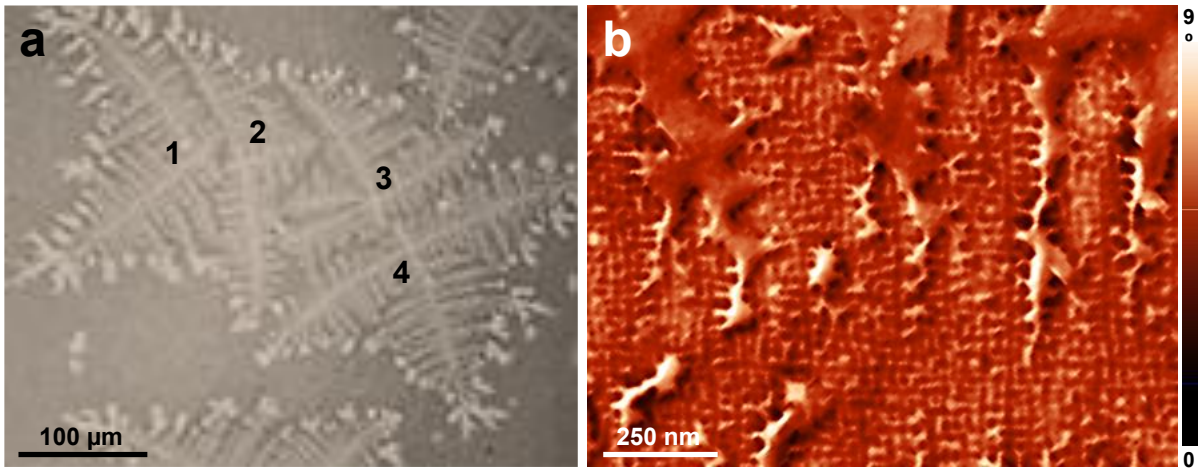

Figure 5.1.2. (a) Optical micrographs illustrating four (partially) coalescing crystals possessing a dendritic structure grown in a thin as spin-cast PB$_{100}$-*b*-P2VP$_{100}$-*b*-PEO$_{104}$ film that was further exposed to toluene vapors via C-SVA. (b) AFM phase micrograph magnified with a 230° rotation corresponding to Figure 5.1.1g highlighting in more detail the presence of interesting substructures measuring in average 16±2 nm in the lateral dimension. This figure was reproduced with permission from ref. [14].

In addition, the average thickness of the dendritic crystal illustrated in Figure 5.1.1c,e was determined by analyzing several cross-sectional profiles obtained by AFM, and was estimated to be approximately 26±5 nm. This value seems to correspond to the thickness of a crystalline PEO lamellae, considering that the maximum length of a PEO chain in the fully extended conformation is about 29 nm (according to the literature, the size of an ethylene oxide monomer

is 0.2783 nm [46]). However, we are not certain whether the crystalline structure penetrates deeper into the 79 nm thick film, below the surface analyzed by AFM.

It is also possible that the semi-crystalline P2VP block contributes to the increase in lamellar thickness by approximately 25 nm (100x0.25 nm [21], [47]). Thus, it cannot be stated with certainty whether the observed crystals consist of folded, tilted, or fully extended molecular chains without further structural analysis based on X-ray diffraction.

However, by comparing the crystal with the neighboring regions in the AFM phase image shown in Figure 5.1.1g, it can be deduced that the stiffness of the crystalline regions was slightly lower than that of the surrounding areas. This result was consistent with the hypothesis that a crystalline material should exhibit a higher stiffness than its amorphous form.

A detailed morphological analysis of the dendritic crystal showed not only that these structures presented, as expected, a complex network of orthogonal branches, but also that these branches included fine, almost perpendicular substructures with an average lateral dimension of approximately 16±2 nm (see the dotted lines in the AFM image in Figure 5.1.1i and the magnification of the substructures in Figure 5.1.2b). To correlate this value with the exact size of the polymer chains and their arrangement within the crystal structure, a full structural investigation using X-ray methods will be required.

References

[1] L. I. Atanase and G. Riess, "Self-assembly of block and graft copolymers in organic solvents: An overview of recent advances," *Polymers*, vol. 10, no. 1, p. 62, 2018.

[2] S. Li, F. Huo, Q. Li, C. Gao, Y. Su, and W. Zhang, "Synthesis of a doubly thermo-responsive schizophrenic diblock copolymer based on poly [N-(4-vinylbenzyl)-N, N-diethylamine] and its temperature-sensitive flip-flop micellization," *Polymer Chemistry*, vol. 5, no. 12, pp. 3910–3918, 2014.

[3] K. Nakashima and P. Bahadur, "Aggregation of water-soluble block copolymers in aqueous solutions: recent trends," *Advances in colloid and interface science*, vol. 123, pp. 75–96, 2006.

[4] G. Riess, "Micellization of block copolymers," *Progress in Polymer Science*, vol. 28, no. 7, pp. 1107–1170, Jul. 2003, doi: 10.1016/S0079-6700(03)00015-7.

[5] I. W. Wyman and G. Liu, "Micellar structures of linear triblock terpolymers: Three blocks but many possibilities," *Polymer*, vol. 54, no. 8, pp. 1950–1978, Apr. 2013, doi: 10.1016/j.polymer.2012.12.079.

[6] A. H. Gröschel and A. H. Müller, "Self-assembly concepts for multicompartment nanostructures," *Nanoscale*, vol. 7, no. 28, pp. 11841–11876, 2015.

[7] J.-N. Marsat, M. Heydenreich, E. Kleinpeter, H. v. Berlepsch, C. Böttcher, and A. Laschewsky, "Self-Assembly into Multicompartment Micelles and Selective Solubilization by Hydrophilic–Lipophilic–Fluorophilic Block Copolymers," *Macromolecules*, vol. 44, no. 7, pp. 2092–2105, Apr. 2011, doi: 10.1021/ma200032j.

[8] S. O. Kyerematen, K. Busse, J. Kohlbrecher, and J. Kressler, “Synthesis and Self-Organization of Poly(propylene oxide)-Based Amphiphilic and Triphilic Block Copolymers,” *Macromolecules*, vol. 44, no. 3, pp. 583–593, Feb. 2011, doi: 10.1021/ma102232z.

[9] Y. Zhang, W. Lin, R. Jing, and J. Huang, “Effect of Block Sequence on the Self-Assembly of ABC Terpolymers in Selective Solvent,” *J. Phys. Chem. B*, vol. 112, no. 51, pp. 16455–16460, Dec. 2008, doi: 10.1021/jp8053444.

[10] L. I. Atanase and G. Riess, “Stabilization of Non-Aqueous Emulsions by Poly(2-Vinylpyridine)-b-Poly(Butadiene) Block Copolymers,” *Colloids Surf. A Physicochem. Eng. Asp.*, vol. 458, pp. 19–24, 2014.

[11] L. I. Atanase and G. Riess, “Micellization of Poly(2-Vinylpyrridine)-b-Poly(Cyclohexyl Methacrylate) (P2VP-b-PCHMA) Block Copolymers and Their Interpolymer Complex Formation in Non-Aqueous Medium,” *J. Colloid Interface Sci.*, vol. 549, pp. 171–178, 2019.

[12] I. Babutan, O. Todor-Boer, L. I. Atanase, A. Vulpoi, S. Simon, and I. Botiz, “Self-assembly of block copolymers on surfaces exposed to space-confined solvent vapor annealing,” *Polymer*, vol. 273, p. 125881, Apr. 2023, doi: 10.1016/j.polymer.2023.125881.

[13] I. Babutan, O. Todor-Boer, L. I. Atanase, A. Vulpoi, and I. Botiz, “Self-Assembly of Block Copolymers in Thin Films Swollen-Rich in Solvent Vapors,” *Polymers*, vol. 15, no. 8, 2023, doi: 10.3390/polym15081900.

[14] I. Babutan, O. Todor-Boer, L. I. Atanase, A. Vulpoi, and I. Botiz, “Crystallization of Poly(ethylene oxide)-Based Triblock Copolymers in Films Swollen-Rich in Solvent Vapors,” *Coatings*, vol. 13, no. 5, 2023, doi: 10.3390/coatings13050918.

[15] I. Babutan, L. I. Atanase, and I. Botiz, “Self-Assembly of Lamellar/Micellar Block Copolymers Induced Through Their Rich Exposure to Various

Solvent Vapors: An AFM Study," *Materials*, vol. 18, no. 8, 2025, doi: 10.3390/ma18081759.

[16] "www.keyence.com/ss/products/measure/sealing/coater-type/spin.jsp."

[17] I. Botiz, N. Grozev, H. Schlaad, and G. Reiter, "The influence of protic non-solvents present in the environment on structure formation of poly(γ-benzyl-l-glutamate) in organic solvents," *Soft Matter*, vol. 4, no. 5, pp. 993–1002, 2008, doi: 10.1039/B719946E.

[18] I. Botiz, H. Schlaad, and G. Reiter, "Processes of Ordered Structure Formation in Polypeptide Thin Film Solutions," in *Self Organized Nanostructures of Amphiphilic Block Copolymers II*, A. H. E. Müller and O. Borisov, Eds., Berlin, Heidelberg: Springer Berlin Heidelberg, 2011, pp. 117–149. doi: 10.1007/12_2010_67.

[19] L. Valentini and M. A. Lopez-Manchado, "Chapter 1 - Classification of rubbers and components for harsh environmental systems," in *High-Performance Elastomeric Materials Reinforced by Nano-Carbons*, L. Valentini and M. A. Lopez Manchado, Eds., Elsevier, 2020, pp. 1–14. doi: 10.1016/B978-0-12-816198-2.00001-3.

[20] J. G. Kennemur, "Poly(vinylpyridine) Segments in Block Copolymers: Synthesis, Self-Assembly, and Versatility," *Macromolecules*, vol. 52, no. 4, pp. 1354–1370, Feb. 2019, doi: 10.1021/acs.macromol.8b01661.

[21] E. A. Lysenko, T. K. Bronich, E. V. Slonkina, A. Eisenberg, V. A. Kabanov, and A. V. Kabanov, "Block Ionomer Complexes with Polystyrene Core-Forming Block in Selective Solvents of Various Polarities. 1. Solution Behavior and Self-Assembly in Aqueous Media," *Macromolecules*, vol. 35, no. 16, pp. 6351–6361, Jul. 2002, doi: 10.1021/ma020048s.

[22] S. Kempf and W. Gronski, "Conductive radical anion salts of poly (butadiene-b-4-vinylpyridine) blockcopolymers," *Polymer Bulletin*, vol. 23, pp. 403–410, 1990.

[23] Q. Wang, X. Zhao, Y.-I. Lee, and H.-G. Liu, "A new and facile way to fabricate catalytically active block copolymer/Au nanoparticle multilayer thin films at the air/liquid interface," *RSC Adv.*, vol. 5, no. 105, pp. 86564–86571, 2015, doi: 10.1039/C5RA16370F.

[24] H.-J. Li and R. C.-C. Tsiang, "Preparation and characterization of a linear poly(4-vinyl pyridine)-b-polybutadiene-b-poly(4-vinylpyridine) using a t-butyllithium/m-diisopropenylbenzene diadduct as a dicarbanion initiator," *Polymer*, vol. 41, no. 15, pp. 5601–5610, Jul. 2000, doi: 10.1016/S0032-3861(99)00810-1.

[25] I. Kudose and T. Kotaka, "Morphological and viscoelastic properties of poly(styrene-b-butadiene-b-4-vinylpyridine) three-block polymers of the ABC type," *Macromolecules*, vol. 17, no. 11, pp. 2325–2332, Nov. 1984, doi: 10.1021/ma00141a022.

[26] Y. Rokhlenko *et al.*, "Magnetic Alignment of Block Copolymer Microdomains by Intrinsic Chain Anisotropy," *Phys. Rev. Lett.*, vol. 115, no. 25, p. 258302, Dec. 2015, doi: 10.1103/PhysRevLett.115.258302.

[27] M. A. Ansarifar and P. F. Luckham, "Measurement of the interaction force profiles between block copolymers of poly(2-vinylpyridine)/poly(t-butylstyrene) in a good solvent," *Polymer*, vol. 29, no. 2, pp. 329–335, Feb. 1988, doi: 10.1016/0032-3861(88)90342-4.

[28] V. P. Chuang, C. A. Ross, J. Gwyther, and I. Manners, "Self-Assembled Nanoscale Ring Arrays from a Polystyrene-b-polyferrocenylsilane-b-poly(2-vinylpyridine)Triblock Terpolymer Thin Film," *Advanced Materials*, vol. 21, no. 37, pp. 3789–3793, Oct. 2009, doi: 10.1002/adma.200900756.

[29] A. J. Marzocca, A. L. Rodríguez Garraza, and M. A. Mansilla, "Evaluation of the polymer–solvent interaction parameter χ for the system cured polybutadiene rubber and toluene," *Polymer Testing*, vol. 29, no. 1, pp. 119–126, Feb. 2010, doi: 10.1016/j.polymertesting.2009.09.013.

[30] V. Narasimhan, R. Y. M. Huang, and C. M. Burns, "Polymer–polymer interaction parameters of polystyrene and polybutadiene from studies in solutions of toluene or tetrahydrofuran," *Journal of Polymer Science: Polymer Physics Edition*, vol. 21, no. 10, pp. 1993–2001, Oct. 1983, doi: 10.1002/pol.1983.180211009.

[31] A. Walther *et al.*, "Multiple Morphologies, Phase Transitions, and Cross-Linking of Crew-Cut Aggregates of Polybutadiene-block-poly(2-vinylpyridine) Diblock Copolymers," *Macromolecules*, vol. 41, no. 9, pp. 3254–3260, May 2008, doi: 10.1021/ma7026148.

[32] X. Gu, I. Gunkel, and T. P. Russell, "Pattern transfer using block copolymers," *Philosophical Transactions of the Royal Society A: Mathematical, Physical and Engineering Sciences*, vol. 371, no. 2000, p. 20120306, Oct. 2013, doi: 10.1098/rsta.2012.0306.

[33] C. G. Arges *et al.*, "Interconnected ionic domains enhance conductivity in microphase separated block copolymer electrolytes," *J. Mater. Chem. A*, vol. 5, no. 11, pp. 5619–5629, 2017, doi: 10.1039/C6TA10838E.

[34] S. Park, B. Kim, A. Cirpan, and T. P. Russell, "Preparation of Metallic Line Patterns from Functional Block Copolymers," *Small*, vol. 5, no. 11, pp. 1343–1348, Jun. 2009, doi: 10.1002/smll.200801409.

[35] J. Lee, J. Kwak, C. Choi, S. H. Han, and J. K. Kim, "Phase Behavior of Poly(2-vinylpyridine)-block-Poly(4-vinylpyridine) Copolymers Containing Gold Nanoparticles," *Macromolecules*, vol. 50, no. 23, pp. 9373–9379, Dec. 2017, doi: 10.1021/acs.macromol.7b01590.

[36] M. S. Rahman, S. Samal, and J.-S. Lee, "Quantitative in Situ Coupling of Living Diblock Copolymers for the Preparation of Amphiphilic Coil−Rod−Coil Triblock Copolymer Poly(2-vinylpyridine)-b-poly(n-hexyl isocyanate)-b-poly(2-vinylpyridine)," *Macromolecules*, vol. 40, no. 26, pp. 9279–9283, Dec. 2007, doi: 10.1021/ma0715730.

[37] Z. Li *et al.*, "Self-Ordering of Diblock Copolymers from Solution," *J. Am. Chem. Soc.*, vol. 118, no. 44, pp. 10892–10893, Jan. 1996, doi: 10.1021/ja961713d.

[38] P. J. Flory, *Principles of polymer chemistry*. Cornell university press, 1953.

[39] H. Tseng, P. Wong, D. R. Lloyd, and J. W. Barlow, "Thermodynamic interaction in polybutadiene/solute systems by inverse gas chromatography," *Polymer Engineering & Science*, vol. 27, no. 15, pp. 1141–1147, 1987.

[40] S. Arichi, H. Matsuura, Y. Tanimoto, and H. Murata, "Studies of Poly-2-vinylpyridine. II. Solubilities in Various Solvents," *Bulletin of the Chemical Society of Japan*, vol. 39, no. 3, pp. 434–439, Mar. 1966, doi: 10.1246/bcsj.39.434.

[41] Z. B. Ren, J. Liu, Y. P. Chen, M. Chen, and D. J. Qian, "Facile fabrication of porous pure and Ag nanoparticle-doped poly(4-vinylpyridine) films at the liquid–liquid interfaces," *Chinese Chemical Letters*, vol. 22, no. 7, pp. 867–870, Jul. 2011, doi: 10.1016/j.cclet.2010.12.042.

[42] J. Raczkowska *et al.*, "Temperature-responsive properties of poly(4-vinylpyridine) coatings: influence of temperature on the wettability, morphology, and protein adsorption," *RSC Adv.*, vol. 6, no. 90, pp. 87469–87477, 2016, doi: 10.1039/C6RA07223B.

[43] T.-M. Chung *et al.*, "Helical Phase Driven by Solvent Evaporation in Self-Assembly of Poly(4-vinylpyridine)-block-poly(l-lactide) Chiral Block Copolymers," *Macromolecules*, vol. 45, no. 24, pp. 9727–9733, Dec. 2012, doi: 10.1021/ma302159p.

[44] C. Darko *et al.*, "Crystallization in diblock copolymer thin films at different degrees of supercooling," *Phys. Rev. E*, vol. 79, no. 4, p. 041802, Apr. 2009, doi: 10.1103/PhysRevE.79.041802.

[45] G. Reiter *et al.*, "Morphologies of Polymer Crystals in Thin Films," in *Progress in Understanding of Polymer Crystallization*, G. Reiter and G. R. Strobl, Eds., Berlin, Heidelberg: Springer Berlin Heidelberg, 2007, pp. 179–200. doi: 10.1007/3-540-47307-6_11.

[46] A. J. Kovacs, C. Straupe, and A. Gonthier, "Isothermal growth, thickening, and melting of polyethylene oxide) single crystals in the bulk. II," *Journal of Polymer Science: Polymer Symposia*, vol. 59, no. 1, pp. 31–54, Jan. 1977, doi: 10.1002/polc.5070590105.

[47] M. Changez, N.-G. Kang, H.-D. Koh, and J.-S. Lee, "Effect of Solvent Composition on Transformation of Micelles to Vesicles of Rod−Coil Poly(n-hexyl isocyanate-block-2-vinylpyridine) Diblock Copolymers," *Langmuir*, vol. 26, no. 12, pp. 9981–9985, Jun. 2010, doi: 10.1021/la100106b.

Annexes

List of ISI publications related to the PhD thesis

1. **I. Babutan,** A.-D. Lucaci, I. Botiz. Antimicrobial Polymeric Structures Assembled on Surfaces. *Polymers* **13**, 1552 (2021). **AIS: 0.657; IF: 4.700.**
2. **I. Babutan,** O. Todor-Boer, L. I. Atanase, A. Vulpoi, S. Simon, I. Botiz. Self-assembly of block copolymers on surfaces exposed to space-confined solvent vapor annealing. Polymer 273, 125881 (2023). **AIS: 0.612; IF: 4.1.**
3. **I. Babutan,** O. Todor-Boer, L. I. Atanase, A. Vulpoi, I. Botiz. Self-Assembly of Block Copolymers in Thin Films Swollen-Rich in Solvent Vapors. Polymers 15, 1900 (2023). **AIS: 0.657; IF: 4.700.**
4. **I. Babutan,** O. Todor-Boer, L. I. Atanase, A. Vulpoi, I. Botiz. Crystallization of Poly(ethylene oxide)-Based Triblock Copolymers in Films Swollen-Rich in Solvent Vapors. Coatings 13, 918 (2023). **AIS: 0.419; IF: 2.900.**
5. **I. Babutan,** L. I. Atanase, I. Botiz, Self-assembly of lamellar/micellar block copolymers induced through their rich exposure to various solvent vapors: an AFM study. Materials 18, 1759 (2025). **AIS: 0.509; IF: 3.100.**

Participation in scientific conferences

6. **I. Babutan,** R. Tarcan, L.-C. Pop, I. Botiz. Poster entitled "Manipulation of the optoelectronic properties of conjugated polymers in thin films by adding reduced graphene oxide" and presented at *International Congress of the Apollonia University of Iasi*, the XXXI edition, hosted by the Apollonia University of Iasi (Romania) on 1st – 3rd March 2021.
7. **I. Babutan,** R. Tarcan, L.-C, Pop, I. Botiz. Oral presentation entitled "Manipulation of optoelectronic properties of conjugated polymers by adding reduced graphene

oxide or silver nanoparticles" and presented at *9th European Young Engineers Conference* in Poland on 19th – 21st of April 2021.

8. **I. Babutan,** R. Tarcan, L.-C. Pop, I. Botiz. Poster entitled "Tuning of the optoelectronic properties of conjugated polymers by the addition of reduced graphene oxide or silver nanoparticles" and presented at *International Conference "Students for Students" XVIIth Edition*, hosted by the Faculty of Chemistry and Chemical Engineering at Babes-Bolyai University of Cluj-Napoca (Romania) on 21st – 24th of April 2021.
9. **I. Babutan,** O. Todor-Boer, L. I. Atanase, I. Botiz. Poster entitled "Fabrication of structured surfaces from antimicrobial copolymers" and presented at *International Congress of the Apollonia University of Iasi*, the XXXIInd edition, hosted by the Apollonia University of Iasi (Romania) on 28th of February – 2nd of March 2022.
10. **I. Babutan,** O. Todor-Boer, L. I. Atanase, A. Vulpoi, S. Simon, I. Botiz. Poster entitled "Self-assembly and crystallization of block copolymers on surfaces exposed to a well-controlled solvent vapor environment and observed by AFM" and presented at virtual offline participation at *Jubilee International Conference on Radiation in Various Fields of Research 10th edition (Jubilee RAD 2022 Conference Summer Edition)* in Herceg Novi (Montenegro) on 25th – 29th of July 2022.
11. **I. Babutan,** O. Todor-Boer, L. I. Atanase, A. Vulpoi, S. Simon, I. Botiz. Poster entitled "Self-assembly of block copolymers on surfaces exposed to space-confined solvent vapor annealing" and presented at *International Congress of the Apollonia University of Iasi*, the XXXIIIth edition, hosted by the Apollonia University of Iasi (Romania) on 2nd – 5th of March 2023.